

Provided for non-commercial research and education use.
Not for reproduction, distribution or commercial use.



(This is a sample cover image for this issue. The actual cover is not yet available at this time.)

This article appeared in a journal published by Elsevier. The attached copy is furnished to the author for internal non-commercial research and education use, including for instruction at the authors institution and sharing with colleagues.

Other uses, including reproduction and distribution, or selling or licensing copies, or posting to personal, institutional or third party websites are prohibited.

In most cases authors are permitted to post their version of the article (e.g. in Word or Tex form) to their personal website or institutional repository. Authors requiring further information regarding Elsevier's archiving and manuscript policies are encouraged to visit:

<http://www.elsevier.com/copyright>

Contents lists available at [SciVerse ScienceDirect](http://www.sciencedirect.com)

Quaternary Science Reviews

journal homepage: www.elsevier.com/locate/quascirev

Global characterization of the Holocene Thermal Maximum

H. Renssen^{a,*}, H. Seppä^b, X. Crosta^c, H. Goosse^d, D.M. Roche^{a,e}^a Department of Earth Sciences, Faculty of Earth and Life Sciences, VU University Amsterdam, Amsterdam, Netherlands^b Department of Geosciences and Geography, University of Helsinki, Helsinki, Finland^c EPOC, UMR 5805, Université Bordeaux 1, CNRS, Talence, France^d Earth and Life Institute, Centre de recherches sur la terre et le climat Georges Lemaître, Université Catholique de Louvain, Louvain-la-Neuve, Belgium^e Laboratoire des Sciences du Climat et de l'Environnement, IPSL, Laboratoire CEA-INSU-UVSQ-CNRS, Gif-sur-Yvette, France

ARTICLE INFO

Article history:

Received 20 December 2011

Received in revised form

24 May 2012

Accepted 29 May 2012

Available online

Keywords:

Holocene

Climate modelling

Global analysis

ABSTRACT

We analyze the global variations in the timing and magnitude of the Holocene Thermal Maximum (HTM) and their dependence on various forcings in transient simulations covering the last 9000 years (9 ka), performed with a global atmosphere-ocean-vegetation model. In these experiments, we consider the influence of variations in orbital parameters and atmospheric greenhouse gases and the early-Holocene deglaciation of the Laurentide Ice sheet (LIS). Considering the LIS deglaciation, we quantify separately the impacts of the background melt-water fluxes and the changes in topography and surface albedo.

In the analysis we focus on the intensity of the maximum temperature deviation relative to the preindustrial level, its timing in the Holocene, and the seasonal expression. In the model, the warmest HTM conditions are found at high latitudes in both hemispheres, reaching 5 °C above the preindustrial level, while the smallest HTM signal is seen over tropical oceans (less than 0.5 °C). This latitudinal contrast is mostly related to the nature of the orbitally-forced insolation forcing, which is also largest at high latitudes, and further enhanced by the polar amplification. The Holocene timing of the HTM is earliest (before 8 ka BP) in regions not affected by the remnant LIS, particularly NW North America, E Asia, N Africa, N South America, the Middle East, NE Siberia and Australia. Compared to the early Holocene insolation maximum, the HTM was delayed by 2–3 ka over NE North America, and regions directly downwind from the LIS. A similar delay is simulated over the Southern Ocean, while an intermediate lag of about 1 ka is found over most other continents and oceans. The seasonal timing of the HTM over continents generally occurs in the same month as the maximum insolation anomaly, whereas over oceans the HTM is delayed by 2–3 months. Exceptions are the oceans covered by sea ice and North Africa, where additional feedbacks results in a different seasonal timing. The simulated timing and magnitude of the HTM are generally consistent with global proxy evidence, with some notable exceptions in the Mediterranean region, SW North America and eastern Eurasia.

© 2012 Elsevier Ltd. All rights reserved.

1. Introduction

The Holocene Thermal Maximum (HTM) was a relatively warm climatic phase between 11 and 5 ka BP, as indicated by numerous proxy records (Kaufman et al., 2004; Jansen et al., 2007, 2008; Wanner et al., 2008; Miller et al., 2010a; Bartlein et al., 2011). The relatively warm conditions during the HTM are commonly associated with the orbitally-forced summer insolation maximum (Wanner et al., 2008; Bartlein et al., 2011). However, proxy records suggest that both the timing and magnitude of maximum warming varied substantially between different regions across the globe, suggesting involvement of additional forcings and feedbacks

(Jansen et al., 2007; Bartlein et al., 2011). One important additional factor affecting the early Holocene climate is the remnant Laurentide Ice sheet (LIS). At mid-to-high latitudes of the Northern Hemisphere, the spatio-temporal complexity of the HTM can be explained by the cooling effect of the LIS, delaying the HTM by 1–2 thousand years compared to the orbitally-forced insolation maximum, particularly in NE North America, the North Atlantic, Western Europe and a zonal band across Eurasia (Kaufman et al., 2004; Kaplan and Wolfe, 2006; Renssen et al., 2009). It is however not clear how the HTM expression at other latitudes relates to orbital forcing and the response to the early Holocene LIS. Although reconstructions of annual-mean temperatures appear to suggest a rather uniform timing of the HTM across the globe (Ljungqvist, 2011), larger differences may exist for different seasons, given the seasonal nature of the orbital forcing.

* Corresponding author. Tel.: +31 20 5987376; fax: +31 20 6462457.

E-mail addresses: h.rensen@vu.nl, hans.rensen@geo.falw.vu.nl (H. Renssen).

Model experiments have shed light on the response of the climate system to orbital forcing during the Holocene. For instance, snapshot simulations performed for 6 ka BP within the framework of the Paleoclimate Modelling Intercomparison Project (PMIP) I and II, suggest that in summer most northern hemisphere continents were about 1–2 °C warmer relative to the preindustrial era due to enhanced summer insolation (Braconnot et al., 2007; Otto et al., 2009; Zhang et al., 2010). Over the oceans, models indicate a less expressed 6–0 ka BP temperature response, varying from +0.5 °C in the North Atlantic Ocean to even a small negative anomaly in the tropical oceans (Braconnot et al., 2007). However, it is likely that simulations for 6 ka BP do not always reflect the conditions during the HTM, as proxy-based reconstructions suggest that the timing of the HTM was much earlier than 6 ka BP at many locations (e.g., Kaufman et al., 2004; Jansen et al., 2007; Bartlein et al., 2011). Moreover, northern hemisphere summer may not have been the season with the largest response in all places (e.g., Davis, 1984).

To improve our understanding of the global expression of the HTM, it is necessary to study the characteristics of the maximum temperature anomaly in transient climate model simulations. In an earlier study (Renssen et al., 2009), we analyzed the HTM at the Northern Hemisphere mid-to-high latitudes, based on a comparison of simulated July temperatures and selected proxy-based reconstructions. In the present paper, we extend this analysis by specifically considering the *global scale*, thereby focusing on the *relative timing of the HTM in different regions*, the *variation in seasonal expression* and the *explanation of these differences*. This focus is expressed in the following questions:

- What is the maximum warming compared to the preindustrial climate?
- What is the timing of the HTM in ka BP?
- What was the seasonal expression of the HTM? In what month of the year is the maximum warm anomaly occurring?
- How consistent are the model-based simulations of the HTM with the proxy-based records?

Our main experiment includes the following forcings: orbital parameters, atmospheric greenhouse gas concentrations, and the impact of the early Holocene Laurentide ice sheet deglaciation (albedo, ice topography and meltwater discharge). By comparing the results of this experiment with those of a simulation with just orbital and greenhouse gas forcing, we are able to analyze the separate impacts of the main forcings. For our analysis, we use the same experiments as discussed in Renssen et al. (2009, 2010).

2. Methods: model and experimental setup

2.1. The model

The model and experimental design have been described in detail in two recent papers (Renssen et al., 2009, 2010), so here only a summary is provided. We performed our simulations with the global ECBilt-CLIO-VECODE3 model. This is an earlier version of the model recently renamed to LOVECLIM, which has been discussed by Goosse et al. (2010). The atmospheric module ECBilt, is a quasi-geostrophic model with T21L3 resolution (Opsteegh et al., 1998), corresponding to ~5.6° latitude by ~5.6° longitude at the surface. The oceanic component CLIO consists of a free-surface, primitive-equation oceanic general circulation model coupled to a dynamic-thermodynamic sea-ice model (Goosse and Fichefet, 1999). CLIO has 20 levels in the vertical and a 3° × 3° latitude-longitude horizontal resolution. Coupled to ECBilt is VECODE; a vegetation model that simulates the dynamics of two main terrestrial plant functional types, trees and grasses, and desert as a dummy type (Brovkin et al.,

2002). ECBilt-CLIO simulates a reasonable present-day climate (Goosse et al., 2001; Renssen et al., 2002). In addition, the response of ECBilt-CLIO-VECODE to mid-Holocene orbital forcing was comparable to that of comprehensive general circulation models (Braconnot et al., 2007). Due to the simplifications in the general circulation equations for the atmosphere, our model has a better performance at mid- and high latitudes than in the tropics (Goosse et al., 2010). This should be kept in mind when interpreting the simulation results. The sensitivity of ECBilt-CLIO to a doubling of the atmospheric CO₂ concentration is within the range of comprehensive GCMs at high latitudes in winter, but slightly weaker at low to mid-latitudes in summer (Petoukhov et al., 2005).

2.2. Experiments

We discuss here two experiments that cover the last 9000 years: ORBGHG and OGMELTICE. These experiments have been discussed before by Renssen et al. (2009, 2010). We started our simulations at 9 ka BP because before that time the influence of the Younger Dryas cold phase, representing major reorganizations of the climate system, may still have had an important impact on climate through the long memory of the deep ocean. Experiment ORBGHG is forced by annually varying values of orbital parameters following Berger (1978), and atmospheric concentrations of the main greenhouse gases CO₂ and CH₄ based on ice core measurements (Raynaud et al., 2000). In ORBGHG, the ice sheets are kept fixed at their present-day configuration. In addition to identical orbital and greenhouse gas forcing as in ORBGHG, in OGMELTICE we also prescribed the impact of the early Holocene LIS deglaciation that lasted until ~6 ka BP. To account for the LIS background melt flux, freshwater was added to the North Atlantic Ocean near the St. Lawrence River Outlet and the Hudson Strait. This additional freshwater flux was adapted from Licciardi et al. (1999) and was set to 0.09 Sv (1 Sv = 10⁶ m³s⁻¹) between 9.0 and 8.4 ka BP, decreasing slightly to 0.08 Sv between 8.4 and 7.8 ka BP, finally dropping to 0.01 Sv between 7.8 and 6.8 ka BP. In OGMELTICE, we also included the impact of the disintegrating LIS during the period 9 to 7 ka BP, by updating surface albedo and topography at 50-year timesteps. The modified surface albedo and topography related to the LIS were based on Peltier (2004), who reconstructed maps of ice sheet extent and thickness since the last glacial maximum (21 ka BP) at 500 year intervals. To obtain the surface albedo and topography at 50-year timesteps, we linearly interpolated in time between the maps provided by Peltier (2004). In both ORBGHG and OGMELTICE, we kept all other forcings (i.e. solar constant, aerosol content) constant at preindustrial values. To obtain initial conditions for OGMELTICE, we spun up the model for 1000 years with 9 ka BP meltwater flux and LIS albedo and topography, starting from a state derived from ORBGHG.

2.3. Insolation

As orbitally-forced changes in insolation are considered the most important driver of long-term Holocene climate change, we discuss here briefly the details of the prescribed insolation. We employed in our model a calendar with 360 days per year, with each month containing 30 days and with the vernal equinox fixed at day 81 (i.e. March 21). This is common practice in Holocene climate modelling studies (e.g., Crucifix et al., 2002; Weber et al., 2004; Braconnot et al., 2007). A calendar with the duration of the months depending on their angular length (Joussaume and Braconnot, 1997) would have been more accurate. However, this would have required major adjustments to the model code that were considered unfeasible within this project.

Within the time-frame considered here, the maximum difference in insolation relative to the preindustrial period is at the very

start (i.e. at 9 ka BP) at all latitudes. In the Northern Hemisphere (NH), at 9 ka BP a positive insolation anomaly was present between about May and August (Fig. 1), peaking in June at values over $+40 \text{ Wm}^{-2}$ north of 60° N (Berger, 1978). In the remainder of the year, a negative 9–0 ka BP insolation anomaly was present in the NH. In the tropics, the positive 9–0 ka BP insolation anomaly was at its smallest with values below $+30 \text{ Wm}^{-2}$, but this rapidly increased towards Southern Hemisphere (SH) high latitudes, with a maximum of $+60 \text{ Wm}^{-2}$ in October South of 80° S . Thus, from north to south, the seasonal timing of the maximum 9–0 ka BP insolation anomaly changed from June to October. Through the Holocene, the timing of this anomaly shifted a bit forwards. For instance, the maximum 4–0 ka positive insolation anomaly occurred in July in the NH and in November in the SH. For the last 9000 years, the annual mean anomaly compared to 0 ka BP was negligible (i.e. within 1 Wm^{-2}) at most latitudes, except for the poles where the maximum was about $+5 \text{ Wm}^{-2}$ at 9 ka BP.

2.4. Analysis of model results

To address the questions raised in the introduction, we analyzed the monthly mean simulation results to establish for each grid cell the *maximum positive temperature anomaly* relative to the preindustrial mean (see example in Fig. 2). The analysis resulted in global maps of this anomaly (Fig. 3a–b), which we consider to represent peak HTM conditions in the model. It is important to note that the anomalies on this map do not represent “real” climatic conditions, as they originate from different months in the year and from different times within the last 9000 years. In addition, we also mapped the *timing of this anomaly in ka BP* (Fig. 4a–b) and the *month of the year* in which this anomaly occurred (Fig. 5). This was done for both ORBGHG and OGMELTICE. The latter experiment is used here as the standard simulation, as it contains the impact of all considered forcings. The preindustrial mean was based on an average over 1000 to 200 yr BP. Before we performed the analysis, we applied a 499-point running mean to all temperatures to filter out high-frequency variability. We have also tested shorter filter lengths of 100 and 250, but these did not sufficiently suppress the impact of unforced variability at multi-centennial scales generated by our model (i.e. in the Southern Ocean). Fig. 2 shows an

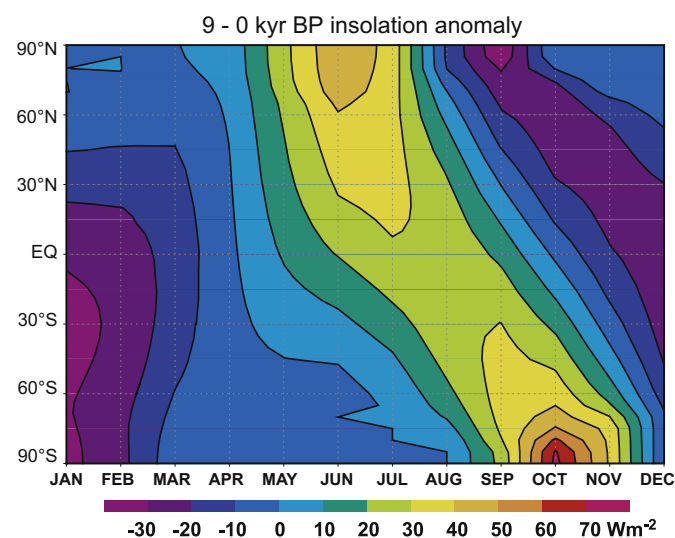


Fig. 1. Difference in monthly insolation values (in Wm^{-2}) between 9 and 0 ka BP for each latitude (based on Berger, 1978).

example of the result of the analysis, with a timing of 7800 yr BP thus meaning that the anomaly averaged over the period 7550–8050 yr BP reached the highest deviation compared to the preindustrial mean.

3. Results

3.1. Simulated global HTM characteristics

3.1.1. What is the maximum warming compared to the preindustrial climate?

Warmest conditions are simulated at high latitudes in both hemispheres, where the anomalies exceed $+5^\circ \text{C}$, whereas smallest positive anomalies (i.e. less than 0.5°C) are found over tropical oceans (Fig. 3a). Over mid-latitude continents, the HTM magnitude is mostly between 1 and 3°C . A marked land-sea contrast is seen at low-to-mid latitudes, with warmest conditions over the continents being $1\text{--}2^\circ \text{C}$ higher than over ocean surfaces at the same latitude.

3.1.2. What is the timing of the HTM in ka BP?

Almost everywhere, the timing of the warmest conditions falls between 9 ka BP and 5 ka BP in OGMELTICE (Fig. 4a). We find the earliest HTM (before 8 ka BP) over NW North America, N South America, Eastern Asia, Northern Africa, the Middle East, Australia, the Central Arctic Ocean and parts of the tropical Pacific and Atlantic Oceans. The latest HTM is simulated over Greenland and along the coast of Arctic Northern Russia, with a timing between 6 and 5 ka BP. In most of Europe and NE North America the timing of the HTM is between 7 and 6 ka BP. A similar HTM timing is found over most of the SH mid-latitudes. In a small region in the equatorial Pacific (green grid cells in Fig. 4a), the timing is notably later (between 4 and 3 ka BP) than the surrounding areas.

3.1.3. In what month of the year is this maximum warming occurring?

Over continents, the timing of the maximum warming occurs later within the seasonal cycle going from north to south (Fig. 5). Over NW North America and Northern Siberia, the maximum warm anomaly falls in June, shifting to July–August over most of continents in the NH mid-latitudes and the tropics. Finally, over land surfaces at SH mid-latitudes, the maximum warm occurs in September–October. Over the oceans a similar latitudinal gradient in seasonal timing exists, but the timing generally lags the terrestrial response by 1–2 months, ranging from August in the North Atlantic to December in the Southern Ocean. Exceptions to this general pattern are the Arctic Ocean, with maximum anomaly in December, part of Northern Africa and Arabia, with maximum warming in April–May, and parts of the Southern Ocean with a timing in July to October.

3.1.4. Summary of the simulated HTM

The main characteristics of the simulated maximum positive temperature deviation from the preindustrial level are presented in Fig. 6 and may be summarized as follows:

- the intensity of the warm anomaly decreases from high to low latitudes,
- at most latitudes, the timing of the maximum deviation is delayed compared to the insolation maximum,
- the spatial difference in Holocene timing is largest at mid-to-high latitudes in the Northern Hemisphere, and
- the seasonal timing of the warm anomaly shifts from NH summer in the north to SH spring (i.e. NH fall) in the south, with a 2–3 month delay over the oceans compared to the continents, with some notable exceptions.

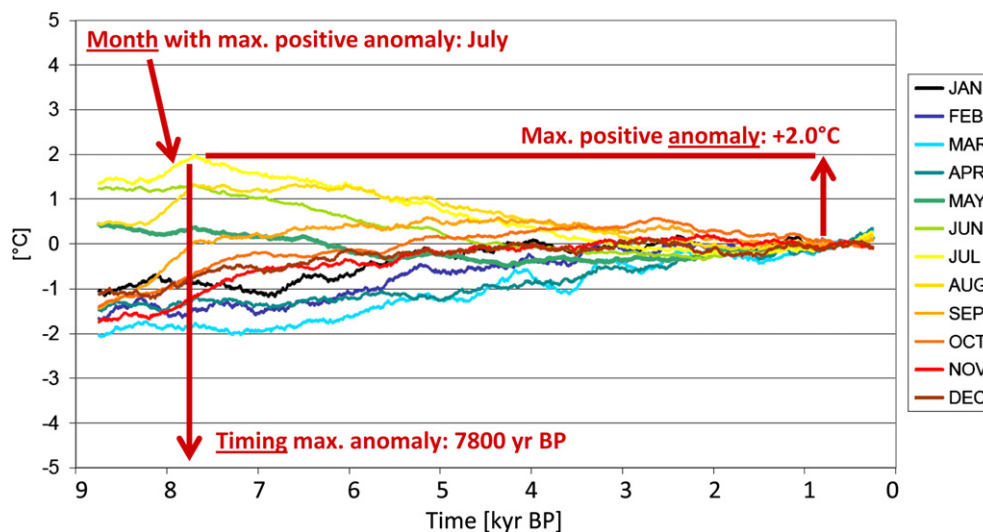


Fig. 2. Example of the analysis performed in this study. The coloured curves are 499-point running averages of simulated monthly surface temperatures in one model grid cell.

4. Discussion of simulated characteristics

4.1. Magnitude of the warming

The contrast in the magnitude of the HTM response between high and low latitudes (Fig. 3a–b) is partly caused by the latitudinal variation in the maximum insolation difference with the preindustrial. This insolation difference also shows a minimum in the tropics and maxima at high latitudes in both hemispheres (Fig. 1). However, the high-latitude HTM response is also stronger because of positive feedbacks, the most prominent ones involving snow and ice, contributing to the well-known polar amplification of climate change (e.g., Holland and Bitz, 2003; Masson-Delmotte et al., 2006; Miller et al., 2010b). When the polar climate warms, the area covered by snow in the winter season becomes less and also the duration of the snow cover is reduced, resulting in an important reduction of the surface albedo and thus to enhanced absorption of shortwave radiation and higher surface temperatures (i.e. the so-called snow-albedo feedback, e.g., Kerwin et al., 1999; Crucifix et al., 2002). The vegetation type also influences the albedo of the snow cover, since it is much higher for tundra and grasslands than for forests (e.g., Harvey, 1988; Foley et al., 2003). In addition, warming of the polar ocean surface waters reduces the thickness of the sea-ice cover, causing the heat flux from the ocean to atmosphere to increase, resulting in additional warming of the lower atmosphere near the surface during the cold season (so-called ice-insulation feedback). Furthermore, previous idealized modelling studies with uniform forcing have indicated that enhanced meridional transport of latent heat in a warmer atmosphere also contributes to polar amplification (e.g., Alexeev et al., 2005; Langen and Alexeev, 2007).

The land-sea contrast in the intensity of the simulated HTM is partly due to the much larger thermal heat capacity of the sea water compared to land surfaces, implying that continents heat up much easier. In addition, compared to land surfaces, oceans also release a relatively large portion of the heat as latent heat, which has no effect on the surface temperature (e.g., Joshi et al., 2008).

4.2. Holocene timing of the HTM

The cooling influence of the early Holocene LIS clearly had a large impact on the global expression of the HTM in our

simulations. Under the influence of the LIS, the early Holocene is relatively cool in many regions in OGMELTICE, not only over the LIS itself (Fig. 4). As discussed previously (Renssen et al., 2009, 2010), the impact of the LIS on the Atlantic Ocean circulation plays an important role in creating these cooler conditions. The background melt flux from the LIS prevents the formation of deepwater in the Labrador Sea in experiment OGMELTICE until around 7 ka BP. Between 9 and 7 ka BP this leads to a reduction of the Atlantic Meridional Overturning Circulation (AMOC) and associated ocean heat transport by about 30%, accompanied by significant cooling of the North Atlantic Ocean, expansion of sea ice and stronger westerly winds relative to ORBGHG. Downwind from the LIS and the cooler North Atlantic Ocean (i.e. much of Europe and a zonal band over Eurasia), this also results in significantly cooler conditions before 7 ka BP. As discussed in detail in Renssen et al. (2010), the relatively cool conditions in the Southern Ocean in OGMELTICE are related to the upwelling of rather cold North Atlantic Deep Water (NADW). The latter is associated with the absence of deep convection in Labrador Sea, leaving the colder Nordic Seas as the only source area of NADW. Consequently, in the early Holocene there was an advective teleconnection in operation between the high latitudes of the Northern and Southern Hemispheres (Renssen et al., 2010).

A comparison to the orbitally-dominated signal in ORBGHG (dark blue in Fig. 4b) shows that in regions with a relatively cool early Holocene under influence of the LIS, the HTM timing is delayed compared to the insolation maximum in OGMELTICE (Fig. 4a). This delay is 1–3 ka over NE North America, most of Europe and a zonal band across Eurasia along 60° N (compare light blue areas Fig. 4a with 4b). A lag of 1–2 ka is also found over most of the Southern Ocean, and the South Pacific. In other regions, such as NW North America, most of the Arctic Ocean and E Asia, the LIS had no discernible impact on the timing of the HTM. A long delay is also suggested in the East Pacific but the signal of the HTM itself is not clear in this region because of the very weak trends simulated by LOVECLIM there.

The map with the difference in the maximum temperature anomaly between OGMELTICE and ORBGHG (Fig. 3b) reflects partly this delay in timing and partly the direct cooling influence of the LIS. In areas that experience a delay in the HTM timing (i.e. between 7 and 6 ka BP instead of between 9 and 8 ka BP) – such as NE North America, the North Atlantic Ocean, Greenland and most of Europe – the cooler conditions are the effect of the reduction in insolation

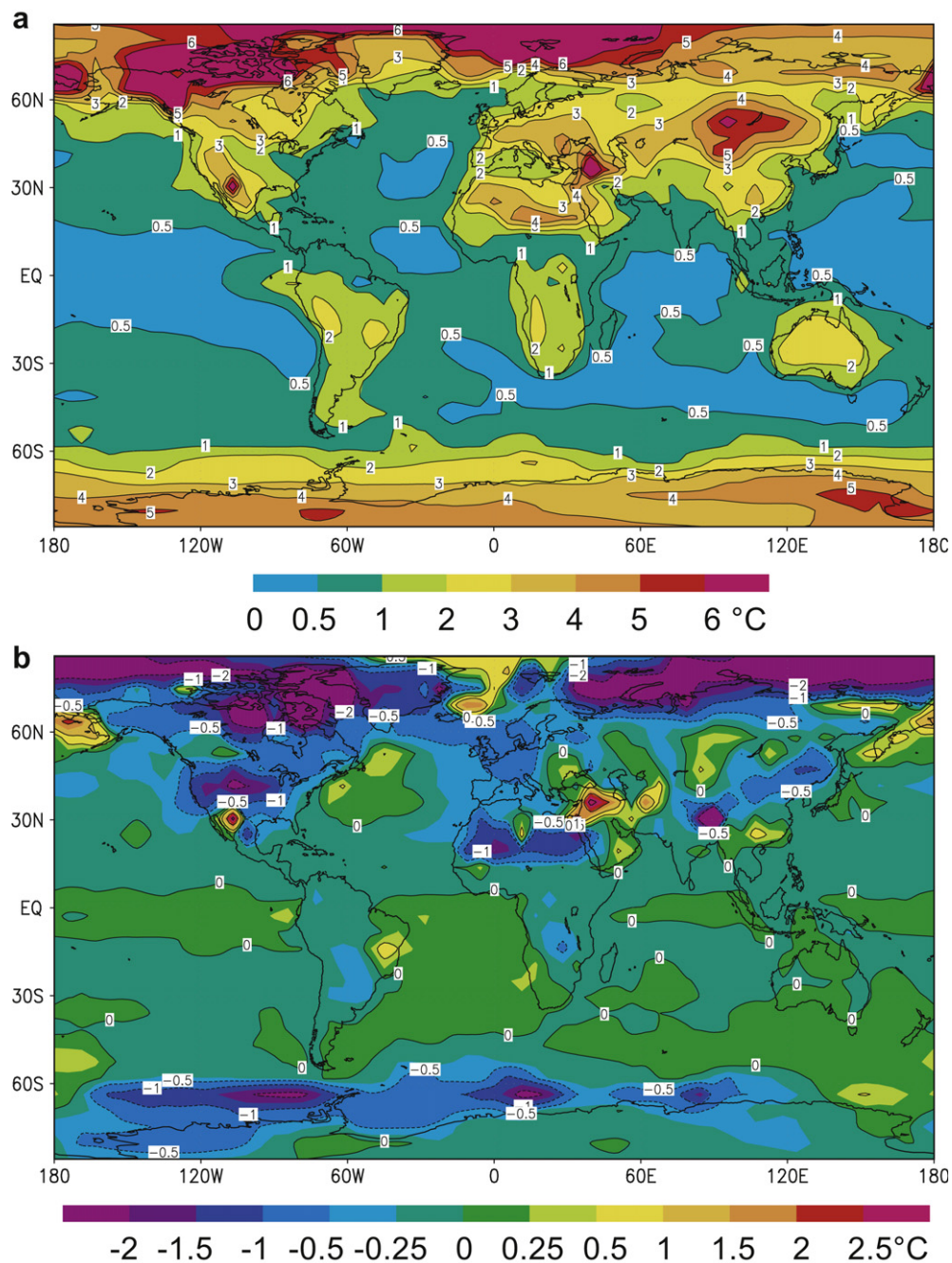


Fig. 3. a (top) and b (bottom): a: Simulated maximum positive surface temperature anomaly in OGMELTICE relative to the preindustrial mean, based on monthly mean results. b: Difference between the maximum positive temperature anomalies in OGMELTICE and ORBGHG.

going from 9 ka BP to 6 ka BP. Over areas without a significant delay – such as NW North America and the Arctic Ocean – the simulated HTM signal is reduced by up to 2 °C due to the LIS influence (Fig. 3b), but here the impact of the orbitally-forced insolation is still stronger than the cooling influence of the LIS, thus resulting in a HTM timing in line with insolation. In southern North America, the cooler HTM conditions are caused by a small shift in the atmospheric circulation that results in an increase in precipitation, leading to moister surface conditions and enhanced evaporation (Fig. 3b).

Compared to ORBGHG, notably warmer HTM conditions in OGMELTICE are seen North of Iceland, the near East and the northernmost Pacific (Fig. 3b). North of Iceland the warmer

conditions are related to a slightly stronger ocean-to-atmosphere heat flux in OGMELTICE that is related to enhanced convective activity (Renssen et al., 2010). In the Near East, reduced precipitation leads to drying of the soil, an enhanced sensible heat flux and relative heating of the surface. Over the northernmost Pacific Ocean, the warm conditions in OGMELTICE are associated with a change in the atmospheric circulation, bringing relatively mild air masses to this region.

The delay of HTM from 9 ka BP to ~7 to 6 ka BP in OGMELTICE also leads to a slight shift within the seasonal cycle in some parts of Europe and NE North America, with the strongest response in August in OGMELTICE compared to July in ORBGHG (not shown).

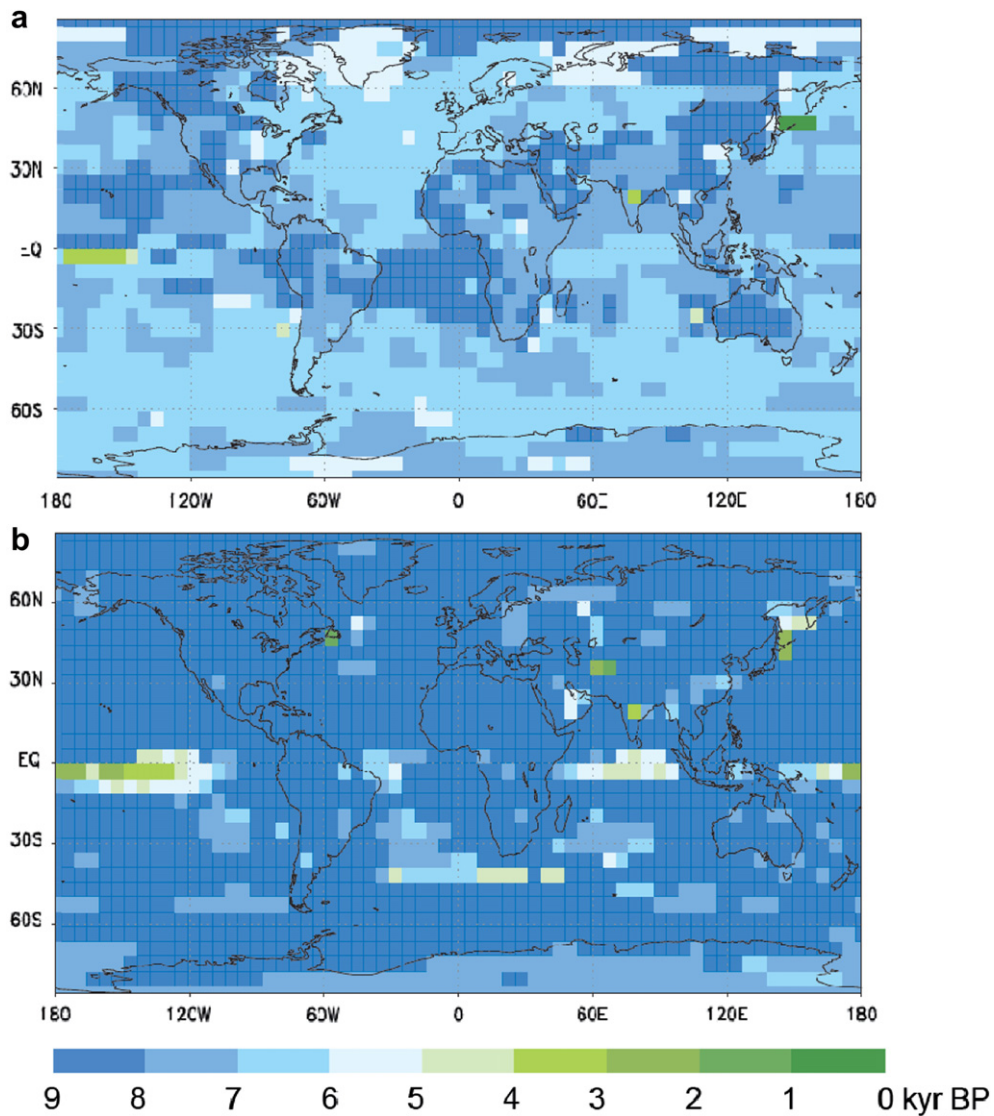


Fig. 4. a (top) and b (bottom): Holocene timing (in ka BP) of the maximum positive temperature anomaly in OGMELTICE (a) and ORBGHG (b).

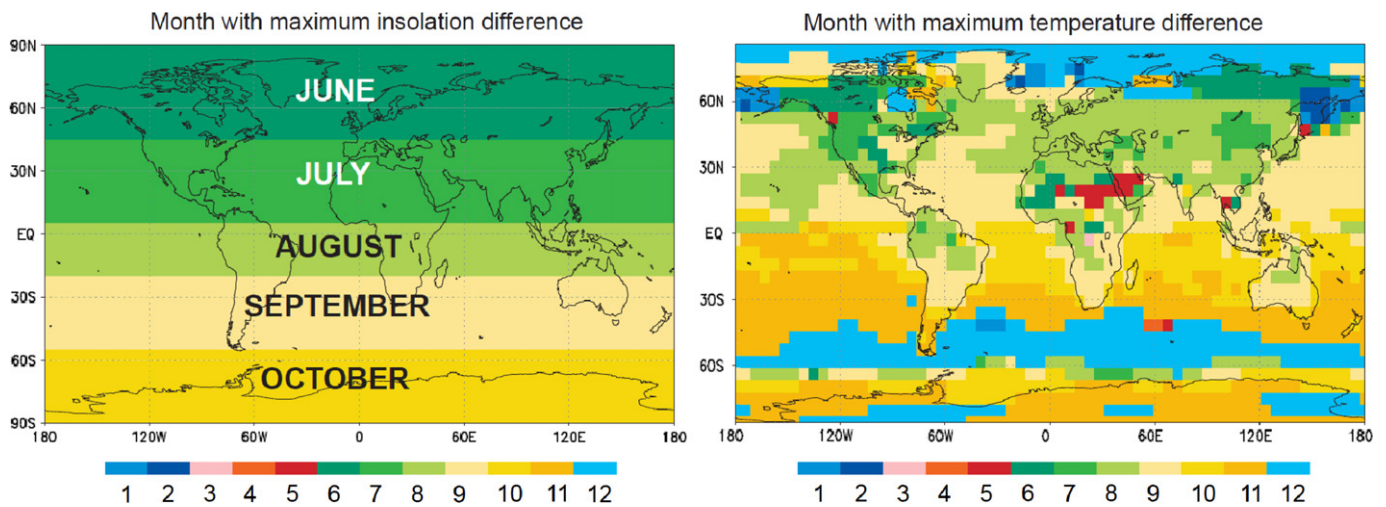


Fig. 5. Month of the year with maximum positive insolation difference at 9 ka BP (left) and the month with the largest positive temperature deviation from the preindustrial mean in OGMELTICE (right).

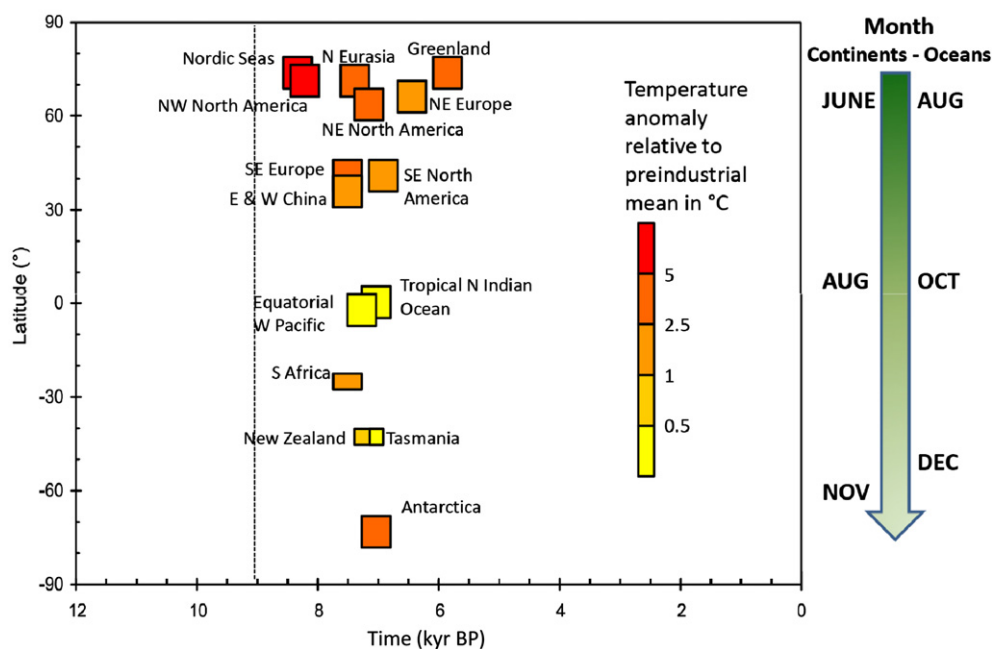


Fig. 6. Summary of main characteristics (Holocene timing, intensity and seasonal timing) of the simulated maximum positive temperature deviation from pre-industrial levels, shown as a function of latitude (vertical axis) and time (horizontal axis). The Holocene timing for the different regions is given with a 500-year range (as indicated by the width of the boxes), consistent with the applied 499-year running mean (see Section 2.4). The green arrow at the right summarizes the seasonal timing of the maximum temperature deviation for the different latitudes. Note that some regions, notably the Arctic and Southern Oceans and North Africa, have a different seasonal expression than indicated by the green arrow (see Section 4.3). Our experiments start at 9 ka BP (indicated by the dashed line), implying that we could not simulate a HTM timing before this time.

This is consistent with the maximum insolation anomaly between 50 and 60° N, which also falls one month later at 7 ka BP than at 9 ka BP.

4.3. Seasonal timing of the HTM

Compared to the continents, the relatively large heat capacity of the oceans is responsible for the greater seasonal lag between the temperature maximum and the insolation maximum over most sea surfaces. The exceptional seasonal timing of the HTM in some regions can be explained by additional processes. The seasonal expression of the simulated HTM over the Arctic Ocean and the Southern Ocean, with the largest anomaly in the winter season, is related to the relatively thin sea-ice cover, enabling the upward ocean heat flux to reach the atmosphere more easily (Fig. 5). In North Africa, the summer insolation anomaly produces enhanced summer monsoons, creating moister conditions that temper the surface heating in summer, resulting in the largest temperature anomalies in spring (i.e. before the summer rains).

4.4. Is the simulated global HTM expression consistent with proxy evidence?

It is difficult to make a meaningful comparison of our simulation results with proxy-based reconstructions of temperature due to associated uncertainties and our discussion will thus remain in many cases qualitative. First, the relation between proxies and temperature is not always direct, and transfer functions often include statistical uncertainties that are 1 °C or more (e.g., Marchal et al., 2002). For many places, this is of the same order of magnitude as the simulated maximum temperature anomaly (Fig. 3a), especially at lower latitudes and over the oceans. Second, different proxies may represent different seasons (e.g., Davis, 1984). For instance, alkenone-based sea-surface temperatures (SSTs) are considered to reflect conditions at the time of maximum coccolith

production, which does not necessarily correspond with the summer conditions reconstructed using diatoms and foraminifera (Marchal et al., 2002), and the continental proxies chironomids are generally seen as a proxy for summer temperatures, whereas pollen records may reflect summer or growing season temperatures, winter temperatures, water balance and other climatic parameters (Huntley, 2011). Third, in many instances the different proxy-based reconstructions are inconsistent, which is most probably related to the two points raised above. As a consequence, it is difficult to obtain a coherent global proxy-based picture of the temporal and spatial of the intensity and timing of the HTM. Jansen et al. (2007, their figure 6.9) made an effort in the 4th assessment report (AR4) of the Intergovernmental Panel on Climate Change (IPCC), but their synthesis was based on only limited amount of available records. To assess whether our simulated global HTM expression is consistent with proxy evidence, we compare in the following sections our results with a selection of proxy-based reconstructions that we consider to provide a fair overview of the global HTM expression in proxy records.

4.4.1. Continental records

For **N Europe**, an earlier model-data comparison suggests that the simulated HTM expression is consistent with proxy-based reconstructions (Davis et al., 2003; Renssen et al., 2009; Seppä et al., 2009). Mid- and high latitude European pollen and chironomid data suggest warmest conditions between 7 and 5 ka BP, with summer temperatures being 0.5–1.5 °C above the preindustrial level. Our model results generally agree well with these data, although the simulation results suggest somewhat warmer summer conditions during the HTM in central Europe (i.e. 3 °C above the preindustrial value). The simulations agree with temperatures based on pollen-climate transfer functions derived from northernmost European Russia, where both methods indicate an HTM magnitude of 3 °C, dating to roughly between 6 and 5 ka BP in the model and between 8 and 3.5 ka BP in the data (Salonen et al., 2011).

Pollen-based summer temperature reconstructions from **Southern Europe** suggest that the early-to-mid Holocene was cooler than the preindustrial period (Davis et al., 2003; Bartlein et al., 2011). This cooler early-to-mid Holocene is not expected from the orbital forcing pattern for summer and is not reproduced by our model. Davis and Brewer (2009) explain this anomalous response by a strong sensitivity of climate to the latitudinal gradients in insolation and temperature. However, the pollen-based temperature reconstructions presented by Davis et al. (2003) for Southern Europe are not unequivocal, as some other reconstructions from this region suggest a long-term Holocene cooling trend (Cheddadi et al., 1998; Marchal et al., 2002; Dormoy et al., 2009), i.e. the opposite response. Using pollen as a temperature proxy in the Mediterranean region might be problematic, since the main climatic parameter influencing plant distribution and vegetation structure here may be effective precipitation rather than temperature (e.g., Osborne et al., 2000). Holocene vegetation changes are therefore interpreted by some researchers as mainly reflecting changes in moisture availability (Jalut et al., 2009). Indeed, relatively large long-term Holocene variations in effective precipitation have been reconstructed in the Mediterranean region using speleothems (Bar-Matthews and Ayalon, 2004) and lake levels (e.g., Cheddadi et al., 1998). Furthermore, late Holocene Mediterranean vegetation has been strongly influenced by human activity and associated changes in fire frequency (e.g., Colombaroli et al., 2009).

Further east, in NE **Siberia**, both model and data indicate that the HTM was significantly earlier, being before 8 ka in the simulation results and between 11.4 and 7.6 ka BP in records from Lake El'gygytyn (Swann et al., 2010). In central Siberia, on the other hand, evidence for the HTM is more ambiguous. The pollen-based reconstructions reported by Bartlein et al. (2011) suggest generally lower-than-present temperatures at 6 ka BP in central Eurasia between 45 and 65° N, whereas Demske et al. (2005) interpret the data from Lake Baikal to show that the HTM appears to have been delayed here too, with a peak warming around 6 ka BP (Demske et al., 2005) that corresponds to a HTM timing between 6 and 8 ka BP in our model.

In **North America**, the model is generally consistent with data. In NE Canada, our model agrees with the pollen-based reconstructions of peak Holocene warming between 7 and 5 ka BP and temperature anomalies of about 1 °C relative to the preindustrial (Kaufman et al., 2004; Kerwin et al., 2004; Renssen et al., 2009; Vau and Gajewski, 2009). Based on numerous proxy data, Kaufman et al. (2004) showed that the HTM timing was between 12 and 8 ka BP in Alaska, which contrasts with a delayed HTM between 7 and 3 ka BP in northernmost Canada. Our simulation suggests a similar contrast in timing, confirming the delaying effect of the LIS in the latter region. In western North America, chironomid-inferred temperatures from the Sierra Nevada in California (Potito et al., 2006) suggest that warmest Holocene conditions were reached at 6.5 ka BP with values of about 2 °C above the present-day level. Our model suggests for this region a similar HTM magnitude, but peaking somewhat earlier between 8 and 7 ka BP. Our model result does contradict pollen-based temperatures from SW North America and the southern part of the continent, showing lower-than-present temperatures at 6 ka BP (Bartlein et al., 2011) and a Holocene warming trend (Vau et al., 2006; Bartlein et al., 2011). However, with reference to the discussion for the Mediterranean region, it could be debated if pollen is an ideal temperature proxy for the semi-arid climate of SW North America.

Proxy records from **Greenland** suggest a considerable variability in the timing and magnitude of the HTM. Oxygen isotope records from the GRIP, GISP2 and NGRIP Greenland ice cores indicate warmest conditions in the earliest Holocene between 9.5 and 7 ka BP (e.g., Johnsen et al., 2001; Thomas et al., 2007; Vinther et al.,

2009), interrupted by the cold 8.2 ka BP event. However, a later timing is indicated by temperature reconstructions based on borehole data from the Dye 3 ice core (between 6 and 3 ka BP) and GRIP (between 8 and 5 ka BP), with anomalies of 2.5–3.0 °C compared to the preindustrial level (Dahl-Jensen et al., 1998). Kaufman et al. (2004) suggest that the HTM warming was stronger at lower elevation sites and locations closer to the ocean than at the summit and high latitudes. This is confirmed by data from several lacustrine records from coastal Greenland (Kaufman et al., 2004). Over most of Greenland, our model simulates a thermal maximum between 6 and 5 ka, which is consistent with some indirect lacustrine evidence for the warmest Holocene conditions in NE Greenland (Klug et al., 2008). Our model also suggests a latitudinal gradient in the HTM magnitude, ranging from 1 °C in the South to 5 °C in the North. Given the low spatial resolution of our model that does not capture the full elevation of the Greenland ice sheet, our simulation results are in reasonable agreement with these reconstructions.

Reviews of proxy-based reconstructions from **China** and the Tibetan Plateau have generally suggested a long period of moister and warmer conditions at 9.5 ka–3 ka BP (Shi et al., 1992; Xiao et al., 2002; Feng et al., 2005; Herzschuh, 2006; Herzschuh et al., 2006; Zhao et al., 2011). In their synthesis of multi-proxy data from a number of sites on the eastern Tibetan Plateau, Zhao et al. (2011) concluded that the maximum warmth was caused by both orbital forcing and monsoon strength, and that the warmest conditions were reached at 6.5 ka BP, followed by gradual cooling and weakening of the monsoon. This is in rough agreement with our simulated HTM between 9 and 7 ka throughout the region. However, more recent investigations have suggested regional asynchronicity in the timing of the highest temperatures and precipitation. For example, He et al. (2004) suggest an early HTM between 11 and 9 ka BP in western China, and a later timing between 9 and 8 ka BP in eastern China and Chen et al. (2008) show that the Holocene climate trends between the monsoonal eastern China and the arid central Asia differ markedly. The monsoonal reconstructions based on stable isotope records from stalagmites (Wang et al., 2005) indicate that the monsoon was strongest in the early Holocene and has attenuated roughly in tune with the summer insolation. It is possible that the strong monsoon suppressed the insolation-induced warming during the early Holocene in northern China, Mongolia and southern Siberia (Bartlein et al., 2011).

In the **Southern Hemisphere mid-latitudes**, evidence seems to confirm that here the HTM was later than would be expected from pure orbital forcing. In New Zealand, Williams et al. (2004) suggested based on speleothem data peak HTM conditions around 10.8 ka BP, and cooler conditions setting in after 7.5 ka BP, while Wilmshurst et al. (2007) found warmest conditions between 9 and 7 ka BP based on pollen, with temperatures being 3–5 °C higher than at present. The timing suggested by the model fits this evidence well, but the simulated peak temperatures for the New Zealand area are less expressed. However, due to the low spatial resolution, the relatively small land mass of New Zealand is not recognized in our model. Speleothem data from Tasmania (Xia et al., 2001) suggest a HTM between 8 and 7 ka BP and pollen-based evidence at 8–5 ka (Fletcher and Thomas, 2007), consistent with the timing in our simulation. In South Africa, proxy evidence suggests that warmest Holocene conditions occurred between about 10.5 and 6 ka BP (Holmgren et al., 2003; Neumann et al., 2010). This is consistent with the modelled peak warming between 9 and 7 ka BP in this region. In southernmost South-America, the HTM occurred at 9–6 ka BP and was characterized by a warming trend that produced warmer and drier conditions than at present in Tierra del Fuego (McCulloch et al., 2000; Waldmann et al., 2010).

Antarctic ice cores (Masson et al., 2000; Jouzel et al., 2001; Masson-Delmotte et al., 2004, 2011) and marine and continental palaeoclimatic records (Bentley et al., 2009) suggest that there were two thermal maxima in Antarctica: one in the earliest Holocene between 11.5 and 9 ka BP, followed by a relatively cold period, and a secondary maximum that varied in timing between 7 and 5 ka BP (Ross Sea sector) and 6–2.5 ka BP (Antarctic Peninsula, Eastern Antarctica). The first thermal maximum is outside the range of our experiments, so we should compare our results with the timing of the secondary optimum. In our simulation, the timing of warmest conditions ranges from 8 to 5 ka BP, in general agreement with the ice-core data. As discussed in Renssen et al. (2010), in OGMELTICE cold conditions prevailed over the Southern Ocean between 9 and 7 ka BP due to the upwelling of relatively cold NADW.

4.4.2. Marine records

North Atlantic sea-surface temperature (SST) reconstructions suggest a thermal maximum in the early to mid Holocene. According to Moros et al. (2004) the HTM lasted until about 6.7 ka BP based on alkenone-based reconstructions, which is consistent with the timing of warmest conditions in our model between 7 and 6 ka BP. Alkenone-based SST reconstructions in the Eastern North Atlantic (Jansen et al., 2008) suggest an increase in the HTM magnitude from less than 1 °C between 20 and 40° N to 2 °C south of Iceland and more than 3 °C in the Nordic Seas north of 65° N. In our model result, this northward increase is of the same order of magnitude. However, SST reconstructions based on diatom assemblages suggest a somewhat earlier and more expressed HTM in the Nordic Seas over the Vøring Plateau, with a 5 °C anomaly compared to the preindustrial level (e.g., Andersen et al., 2004; Berner et al., 2011), and a timing between 9 and 7 ka BP, revealing a clear mismatch with the alkenone-based reconstructions (Marchal et al., 2002). This might reflect the already noted difference in seasonal representation between the two methods (i.e. annual in alkenone based SSTs, summer in diatom-based SSTs). Southwest of Iceland, the diatom-based reconstructions indicate a later HTM between 6 and 5 ka BP, with a magnitude of 1–2 °C (Berner et al., 2008), fully consistent with alkenones (Marchal et al., 2002; Jansen et al., 2008) and our model results.

In **tropical oceans**, the HTM signal appears to be small, and there is some conflicting evidence of the trend of ocean surface temperatures over the Holocene. In the Western Tropical Pacific, Stott et al. (2004) derived 0.5 °C warmer conditions during the early part of the Holocene (between 10 and 5 ka BP) based on foraminiferal oxygen isotope and Mg/Ca data, corresponding well with our results. However, most tropical alkenone SST records (Rimbu et al., 2004; Lorenz et al., 2006) suggest a warming trend over the entire Holocene and cooler than present conditions between 9 and 6 ka BP, although there are some notable exceptions (e.g., Kim et al., 2003). Our model does not reproduce this overall warming trend, and suggests that temperatures were warmer than today at some point in the Holocene, also in the annual mean (not shown). It should be noted that over tropical oceans the warm anomaly in the model is small (less than 0.5 °C). Only in a small area of the equatorial Pacific (indicated by green grid cells in Fig. 4a), the simulated temperatures are cooler than today between 9 and 6 ka BP. The noted general pattern of Holocene warming observed in alkenone-derived SSTs is not reproduced in the overall picture emerging from SST reconstructions based on Mg/Ca ratios (Leduc et al., 2010). For instance, in the tropical Atlantic off Congo, a Mg/Ca-derived reconstruction by Weldeab et al. (2007) suggests warmest Holocene SSTs (~1.5 °C above late Holocene level) between 10 and 8 ka BP, followed by a cooling trend. Several explanations have been proposed for the mismatch between alkenones and Mg/Ca ratios,

including different seasonal representations for both methods (see Leduc et al., 2010 for a detailed discussion).

Alkenone-based SST reconstructions for many marine cores in the **North Pacific Ocean** also suggest a small Holocene warming trend (Kim et al., 2004), ranging from 0.3 to 1.8 °C increase over the last 7 ka. However, at some sites in the N Pacific, alkenone-based SSTs show a slight long-term cooling, thus contrasting with the warming trend in the majority of the alkenone records here (Kim et al., 2004). A clear HTM, followed by a cooling trend, is also suggested by radiolarian-based SST reconstructions from the East China Sea (Fengming et al., 2008). Our model does simulate a small cooling trend of 0.5–1 °C over the last 7 ka, and thus provides no support for cooler surface conditions in the mid-Holocene N Pacific. As mentioned above, alkenone-based SST reconstructions reflect the period of maximum coccolith production, and it may not always be clear what season this represents and if this has been stable throughout the Holocene, thus complicating model-data comparisons.

In the **Southern Ocean**, proxy records indicate a complex temporal structure of the changes over the Holocene. Some coastal records support our modelled HTM timing that falls mostly 7 and 6 ka BP. For instance, coastal diatom records sampled near East Antarctica also reveal a cooler phase between 9 and 7.5 ka BP with extended sea-ice cover, followed by warmer conditions lasting until about 4 ka BP (Crosta et al., 2007, 2008; Denis et al., 2009, 2010). However, a variety of responses has been recorded in eastern Antarctica, as reviewed by Wagner and Melles (2007), suggesting a quite complex structure of the changes over the Holocene here. Also, marine diatom records from the Atlantic sector south of the polar front, suggest earlier warmest conditions between 12 and 9 ka BP, followed by cooling and sea ice expansion between 9 and 7 ka BP (Bianchi and Gersonde, 2004), in agreement with the Antarctic ice core records. A recent SST reconstruction based on the TEX86 methodology from a core west of the Antarctic Peninsula confirms warmest conditions between 12 and 8 ka BP (Shevenell et al., 2011). Other records from the Antarctic Peninsula indicate a later thermal maximum, for instance between 9 and 7 ka BP (e.g., Brachfeld et al., 2002; Sjunneskog and Taylor, 2002; Roberts et al., 2008) and or even between 8–7 and 4–3 ka BP (Taylor et al., 2001; Heroy et al., 2008). As discussed in detail by Denis et al. (2010), the coastal signature of warmest conditions in the first half of the Holocene contrasts with the response of the open ocean in the East Atlantic and Indian Ocean sectors that suggests relatively cool conditions until 4.5–3.5 ka BP, followed by warming (Hodell et al., 2001; Nielsen et al., 2004; Anderson et al., 2009). Denis et al. (2010) relate this latitudinal contrast to a strong sensitivity to the latitudinal temperature gradient.

4.5. Is the HTM an analogue for the climate at the end of the 21st century?

There are some similarities between the AR4 projections of the IPCC (Meehl et al., 2007, Fig. 10.9) for the end of the 21st Century and our simulation results for the HTM. First, in both cases, similar warm conditions are present over the Arctic Ocean during the winter season. Our simulated December temperature anomalies of more than 6 °C are comparable to the AR4 winter projection between 6.5 °C to more than 7.5 °C in the A1B scenario. Second, over Northern Hemisphere high and mid-latitude continents, the largest response is in summer, with comparable temperature anomalies between 2 and 5 °C in both our simulation and the AR4 results for the A1B scenario. However, over mid-to-low latitude the oceans, the HTM anomaly is smaller in our model (0.5–1 °C) compared to the 1–2 °C warming suggested by AR4. It should be noted that our model's sensitivity to radiative forcing is slightly

weaker than comprehensive GCMs at low to mid latitudes in summer (Petoukhov et al., 2005), implying that the comparison to AR4 results is not always straightforward.

In any case, important differences between the two periods exist in the duration and the spatiotemporal variability. The future climate conditions from AR4 discussed above refer to only two decades at the end of the 21st Century. Moreover, the AR4 projections suggest that it will be a period with rapid climate warming that is likely followed by even warmer conditions in the subsequent decades. The HTM, on the other hand, reflects more or less stable conditions during at least a millennium. The HTM is also a time-transgressive phenomenon, with much larger spatiotemporal variations than projected for the 21st Century. Both our model results and proxy evidence suggest that the timing of the HTM in different regions differs by as much as 3000 years, even at the same latitude. In addition, we have only considered the temperature response here, and it is likely that there also notable differences in other climate characteristics between the two periods (e.g., in precipitation). In summary, there are some similarities between the HTM and the projected climate at the end of the 21st Century, particularly with respect to the magnitude of the warming and the seasonal characteristics in the Arctic/Subarctic regions as was also discussed by MacDonald (2010), but important differences in duration and spatiotemporal variability between the two periods imply that the HTM is not a close analogue for the predicted global warming by the end of the 21st Century.

5. Conclusions

We analyzed transient climate model simulations of the last 9000 years to characterize the HTM in terms of the maximum positive temperature anomaly, the timing of this anomaly and the month of the year with the strongest response. Our analysis suggests the following.

- The HTM expression was strongest at high latitudes in both hemispheres, where the maximum temperature anomaly relative to the preindustrial reached 5 °C in our model. The weakest HTM signal was simulated over low-latitude oceans (less than 0.5 °C) and low latitude continents (0.5–1.5 °C). Over mid-to-high latitude continents the HTM anomaly was between 1 and 4 °C.
- This latitudinal contrast is partly caused by the orbitally-forced insolation anomaly that is also largest at high latitudes. The strong high-latitude response is amplified by polar amplification.
- The earliest HTM (before 8 ka BP) is found in regions not affected by the remnant early Holocene Laurentide Ice sheet. Most notably, this is the case in NW North America, E Asia, N Africa, N South America, the Middle East, NE Siberia, and Australia. Compared to the insolation maximum, the HTM was delayed by 2–3 ka over NE North America (i.e. location of LIS) and regions directly downwind from the LIS, i.e. North Atlantic, Greenland, Europe, and a zonal band across Asia. This was also apparent over much of the Southern Ocean. An intermediate delay of around 1 ka was found over most other continents and oceans.
- One implication of this temporal heterogeneity of the HTM timing is that the 6 ka BP climate cannot be used as a good representation of the HTM climate, as is sometimes assumed in modelling studies.
- The seasonal expression of the HTM is such that over continents the maximum positive temperature anomaly generally occurred in the same month as the maximum insolation anomaly. Over ocean surfaces, the timing of the HTM within

the seasonal cycle was delayed by 2–3 months relative to the insolation maximum. Exceptions are found in the Arctic Ocean, North Africa and the Southern Ocean. Over the Arctic Ocean and the Southern Ocean, the largest anomaly is simulated in winter, when the thinner sea ice allows for a relatively strong upward heat flux from the ocean. In North Africa, the summer insolation anomaly leads to enhanced summer monsoon, creating moister conditions that temper the surface heating in summer, resulting in the largest temperature anomalies in spring (i.e. before the rains).

- The timing and magnitude of the HTM in our model results is generally consistent with global proxy evidence, indicating that our simulations provide a reasonable global characterization of the HTM.
- Regions where there are clear mismatches between model and data include the Mediterranean region, SW North America, northern China, Mongolia and southern Siberia, and some ocean regions (alkenone SSTs in tropics and N Pacific). It is possible that that in these instances the reconstruction-methods may not be suitable to reconstruct temperature conditions during the HTM, but it is also possible that the model simulations are unable to capture all the second order components of past climate systems (e.g., circulation changes) and, hence, give incorrect simulation results in these regions. We suggest that model-based and proxy-based palaeoclimatological research should focus on these regions in the future.
- The HTM represents the most recent major geological warm period and it is thus a potential analogue for the warmer climate projected for the end of the 21st Century. However, although there are some similarities, particularly with respect to the warming and the seasonal characteristics in the Arctic/Subarctic regions, important differences in duration and spatiotemporal variability have been identified in the HTM. Most importantly, the HTM does not represent a globally coherent and synchronous warm period, making it a poorly suitable reference climate for the future climate for most of the world.

Acknowledgements

This is Past4Future contribution number 18. The research leading to these results has received funding from the European Union's Seventh Framework programme (FP7/2007-2013) under grant agreement number 243908, "Past4Future. Climate change - Learning from the past climate". This is also a contribution (number 9) to the HOLOCLIP Project, a joint research project of ESF Polar-CLIMATE programme, which is funded by national contributions from Italy, France, Germany, Spain, Netherlands, Belgium and the United Kingdom. HS acknowledges the financial support from the Nordic top-level research initiative CRAICC. DMR is funded by the NWO under project number 854.00.024 and by INSU-CNRS

References

- Alexeev, V.A., Langen, P.L., Bates, J.R., 2005. Polar amplification of surface warming on an aquaplanet in "ghost forcing" experiments without sea ice feedbacks. *Climate Dynamics* 24, 655–666.
- Andersen, C., Koç, N., Jennings, J., Andrews, J.T., 2004. Nonuniform response of the major surface currents in the Nordic Seas to insolation forcing: implications for the Holocene climate variability. *Paleoceanography* 19, PA2003. <http://dx.doi.org/10.1029/2002PA000873>.
- Anderson, R.F., Ali, S., Bradtmiller, L.I., Nielsen, S.H.H., Fleisher, M.Q., Anderson, B.E., Burckle, L.H., 2009. Wind-driven upwelling in the Southern Ocean and the deglacial rise in atmospheric CO₂. *Science* 323, 1443–1448.
- Bar-Matthews, M., Ayalon, A., 2004. Speleothems as palaeoclimatic indicators, a case study from Soreq Cave located in the Eastern Mediterranean Region,

- Israel. In: Battarbee, R.W., Gasse, F., Stickley, C.E. (Eds.), *Past Climate Variability Through Europe and Africa*. Springer, Dordrecht, The Netherlands, pp. 363–391.
- Bartlein, P.J., Harrison, S.P., Brewer, S., Connor, S., Davis, B.A.S., Gajewski, K., Guiot, J., Harrison-Prentice, T.I., Henderson, A., Peyron, O., Prentice, I.C., Scholze, M., Seppä, H., Shuman, B., Sugita, S., Thompson, R.S., Viau, A.E., Williams, J., Wu, H., 2011. Pollen-based continental climate reconstructions at 6 and 21 ka: a global synthesis. *Climate Dynamics* 37, 755–802.
- Bentley, M.J., Hodgson, D.A., Smith, J.A., Cofaigh, C.Ó., Domack, E.W., Larter, R.D., Roberts, S.J., Brachfeld, S., Leventer, A., Hjort, C., Hillenbrand, C.-D., Evans, J., 2009. Mechanisms of Holocene palaeoenvironmental change in the Antarctic Peninsula region. *The Holocene* 19, 51–69.
- Berger, A.L., 1978. Long-term variations of daily insolation and Quaternary climatic changes. *Journal of the Atmospheric Sciences* 35, 2363–2367.
- Berner, K.S., Koc, N., Divine, D., Godtliessen, F., Moros, M., 2008. A decadal-scale Holocene sea surface temperature record from the subpolar North Atlantic constructed using diatoms and statistics and its relation to other climate parameters. *Paleoceanography* 23, PA2210. <http://dx.doi.org/10.1029/2006PA001339>.
- Berner, K.S., Koc, N., Godtliessen, F., Divine, D., 2011. Holocene climate variability of the Norwegian Atlantic Current during high and low solar insolation forcing. *Paleoceanography* 26, PA2220. <http://dx.doi.org/10.1029/2010PA002002>.
- Bianchi, P., Gersonde, R., 2004. Climate evolution at the last deglaciation: the role of the Southern Ocean. *Earth and Planetary Science Letters* 228, 407–424.
- Brachfeld, S.A., Banerjee, S.K., Guyodo, Y., Acton, G.D., 2002. A 13 200 year history of century to millennial-scale paleoenvironmental change magnetically recorded in the Palmer Deep, western Antarctic Peninsula. *Earth and Planetary Science Letters* 194, 311–326.
- Braconnot, P., Otto-Bliesner, B., Harrison, S., Joussaume, S., Peterschmitt, J.-Y., Abe-Ouchi, A., Crucifix, M., Driesschaert, E., Fichet, Th., Hewitt, C.D., Kageyama, M., Kitoh, A., Lâiné, A., Loutre, M.-F., Marti, O., Merkel, U., Ramstein, G., Valdes, P., Weber, S.L., Yu, Y., Zhao, Y., 2007. Results of PMIP2 coupled simulations of the mid-Holocene and Last Glacial maximum – Part 1: experiments and large-scale features. *Climate of the Past* 3, 261–277.
- Brovkin, V., Bendtsen, J., Claussen, M., Ganopolski, A., Kubatzki, C., Petoukhov, V., Andreev, A., 2002. Carbon cycle, vegetation and climate dynamics in the Holocene: experiments with the CLIMBER-2 model. *Global Biogeochemical Cycles* 16, 1139. <http://dx.doi.org/10.1029/2001GB001662>.
- Cheddadi, R., Lamb, H.F., Guiot, J., van der Kaars, S., 1998. Holocene climatic change in Morocco: a quantitative reconstruction from pollen data. *Climate Dynamics* 14, 883–890.
- Chen, F., Yu, Z., Yang, M., Ito, E., Wang, S., Madsen, D.B., Huang, X., Zhao, Y., Sato, T., Birks, H.J.B., Boomer, I., Chen, J., An, C., Wünnemann, B., 2008. Holocene moisture evolution in arid central Asia and its out-of-phase relationship with Asian monsoon history. *Quaternary Science Reviews* 27, 351–364.
- Colombaroli, D., Tinner, W., van Leeuwen, J., Noti, R., Vecoví, E., Vanniere, B., Magny, M., Schmidt, R., Bugmann, H., 2009. Response of broadleaved evergreen Mediterranean forest vegetation to fire disturbance during the Holocene: insights from the peri-Adriatic region. *Journal of Biogeography* 36, 314–326.
- Crosta, X., Debret, M., Denis, D., Courty, M.A., Ther, O., 2007. Holocene long- and short-term climate changes off Adélie Land, East Antarctica. *Geochemistry, Geophysics, Geosystems* 8, Q11009. <http://dx.doi.org/10.1029/2007GC001718>.
- Crosta, X., Denis, D., Ther, O., 2008. Sea ice seasonality during the Holocene, Adélie Land, East Antarctica. *Marine Micropaleontology* 66, 222–232.
- Crucifix, M., Loutre, M.F., Tulkens, P., Fichet, T., Berger, A., 2002. Climate evolution during the Holocene: a study with an Earth system model of intermediate complexity. *Climate Dynamics* 19, 43–60.
- Dahl-Jensen, D., Mosegaard, K., Gundestrup, N., Clow, G.D., Johnsen, S.J., Hansen, A.W., Balling, N., 1998. Past temperatures directly from the Greenland ice sheet. *Science* 282, 268–271.
- Davis, B.A.S., Brewer, S., 2009. Orbital forcing and role of the latitudinal insolation/temperature gradients. *Climate Dynamics* 32, 143–165.
- Davis, B.A.S., Brewer, S., Stevenson, A.C., Guiot, J., Data Contributors, 2003. The temperature of Europe during the Holocene reconstructed from pollen data. *Quaternary Science Reviews* 22, 1701–1716.
- Davis, O.K., 1984. Multiple thermal maxima during the Holocene. *Science* 225, 617–619.
- Demske, D., Heumann, G., Granoszewski, W., Nita, M., Mamakowa, K., Tarasov, P.E., Oberhänsli, H., 2005. Late glacial and Holocene vegetation and regional climate variability evidenced in high-resolution pollen records from Lake Baikal. *Global and Planetary Change* 46, 255–279.
- Denis, D., Crosta, X., Schmidt, S., Damien, C., Raja, G., Renssen, H., Bout-Roumazeilles, V., Zaragosi, S., Bernard, M., Giraudeau, J., 2009. Glacier and deep water Holocene dynamics, Adélie Land region, East Antarctica. *Quaternary Science Reviews* 28, 1291–1303.
- Denis, D., Crosta, X., Barbara, L., Massé, G., Renssen, H., Ther, O., Giraudeau, J., 2010. Sea ice and wind variability during the Holocene in East Antarctica: insight on middle-high latitude coupling. *Quaternary Science Reviews* 29, 3709–3719.
- Dormoy, I., Peyron, O., Combourieu Nebout, N., Goring, S., Kotthoff, U., Magny, M., Pross, J., 2009. Terrestrial climate variability and seasonality changes in the Mediterranean region between 15 000 and 4000 years BP deduced from marine pollen records. *Climate of the Past* 5, 615–632.
- Feng, Z.-D., An, C.B., Wang, H.B., 2005. Holocene climatic and environmental changes in the arid and semi-arid areas of China: a review. *The Holocene* 16, 119–130.
- Fengming, C., Li, T., Zhuang, L., Yan, J., 2008. A Holocene paleotemperature record based on radiolaria from the northern Okinawa Trough (East China Sea). *Quaternary International* 183, 115–122.
- Fletcher, M.-S., Thomas, I., 2007. Holocene vegetation and climate change from near Lake Peddler, south-west Tasmania, Australia. *Journal of Biogeography* 34, 665–677.
- Foley, J.A., Heil Costa, M., Delire, C., Ramankutty, N., Snyder, P., 2003. Green surprise? How terrestrial ecosystems could affect earth's climate. *Frontiers in Ecology and the Environment* 1, 38–44.
- Goosse, H., Fichet, T., 1999. Importance of ice-ocean interactions for the global ocean circulation: a model study. *Journal of Geophysical Research* 104, 23,337–23,355.
- Goosse, H., Seltin, F.M., Haarsma, R.J., Opsteegh, J.D., 2001. Decadal variability in high northern latitudes as simulated by an intermediate-complexity climate model. *Annals of Glaciology* 33, 525–532.
- Goosse, H., Brovkin, V., Fichet, T., Haarsma, R., Huybrechts, P., Jongma, J., Mouchet, A., Seltin, F., Barriat, P.-Y., Campin, J.-M., Deleersnijder, E., Driesschaert, E., Goelzer, H., Janssens, I., Loutre, M.-F., Maqueda, M.A., Opsteegh, T., Mathieu, P.-P., Munhoven, G., Pettersson, E.J., Renssen, H., Roche, D.M., Schaeffer, M., Tartinville, B., Timmermann, A., Weber, S.L., 2010. Description of the Earth system model of intermediate complexity LOVECLIM version 1.2. *Geoscientific Model Development* 3, 603–633.
- Harvey, L.D.D., 1988. On the role of high latitude ice, snow, and vegetation feedbacks in the climatic response to external forcing changes. *Climatic Change* 13, 191–224.
- He, Y., Theakstone, W.H., Zhang, Z., Zhang, D., Yao, T., Chen, T., Shen, Y., Pang, H., 2004. Asynchronous Holocene climatic change across China. *Quaternary Research* 61, 52–63.
- Heroy, D.C., Sjunneskog, C., Anderson, J.B., 2008. Holocene climate change in the Bransfield Basin, Antarctic Peninsula: evidence from sediment and diatom analysis. *Antarctic Science* 20, 69–87.
- Herzschuh, U., Winter, K., Wünnemann, B., Li, S., 2006. A general cooling trend on the central Tibetan Plateau throughout the Holocene recorded by the Lake Zigetang pollen spectra. *Quaternary International* 154–155, 113–121.
- Herzschuh, U., 2006. Palaeo-moisture evolution in monsoonal Central Asia during the last 50,000 years. *Quaternary Science Reviews* 25, 164–178.
- Hodell, D.A., Kanfoush, S.L., Shemesh, A., Crosta, X., Charles, C.D., Guilderson, T.P., 2001. Abrupt cooling of Antarctic Surface waters and sea ice expansion in the South Atlantic sector of the Southern Ocean at 5000 cal yr BP. *Quaternary Research* 56, 191–198.
- Holland, M.M., Bitz, C.M., 2003. Polar amplification of climate change in coupled models. *Climate Dynamics* 21, 221–232.
- Holmgren, K., Lee-Thorp, J.A., Cooper, G.R.J., Lundblad, K., Partridge, T.C., Scott, L., Sitaldeen, R., Talma, A.S., Tyson, P.D., 2003. Persistent millennial-scale climatic variability over the past 25,000 years in Southern Africa. *Quaternary Science Reviews* 22, 2311–2326.
- Huntley, B., 2011. Reconstructing palaeoclimates from biological proxies. Some often overlooked sources of uncertainty. *Quaternary Science Reviews*. <http://dx.doi.org/10.1016/j.quascirev.2011.11.006>.
- Jalut, G., Dedouat, J.J., Fontugne, M., Otto, T., 2009. Holocene circum-Mediterranean vegetation changes: climate forcing and human impact. *Quaternary International* 200, 4–18.
- Jansen, E., Overpeck, J.T., Briffa, K.R., Duplessy, J.C., Joos, F., Masson-Delmotte, V., Olago, D., Otto-Bliesner, B., Peltier, W.R., Rahmstorf, S., Rengaswamy, R., Raynaud, D., Rind, D., Solomina, O., Villalba, R., Zhang, D., 2007. Palaeoclimate. In: Solomon, S., Qin, D., Manning, M., Chen, Z., Marquis, M., Averyt, K.B., Tignor, M., Miller, H.L. (Eds.), *Climate Change 2007: the Physical Science Basis*. 4th Assessment Report IPCC. Cambridge Univ. Press, Cambridge, UK, pp. 433–498.
- Jansen, E., Andersson, C., Moros, M., Nisancioglu, K.H., Nyland, B.F., Telford, R.J., 2008. The early to mid-Holocene thermal optimum in the North Atlantic. In: Battarbee, R.W., Binney, H.A. (Eds.), *Natural Climate Variability and Global Warming: a Holocene Perspective*. Wiley-Blackwell, Chichester, pp. 123–137.
- Johnsen, S.J., Dahl-Jensen, D., Gundestrup, N., Stefansen, J.P., Clausen, H.B., Miller, H., Masson-Delmotte, V., Sveinbjörnsdóttir, A.E., White, J., 2001. Oxygen isotope and palaeotemperature records from six Greenland ice core stations: camp century, Dye-3, GRIP, GISP2, Renland and NorthGRIP. *Journal of Quaternary Science* 16, 299–307.
- Joshi, M.M., Gregory, J.M., Webb, M.J., Sexton, D.M.H., Johns, T.C., 2008. Mechanisms for the land/sea warming contrast exhibited by simulations of climate change. *Climate Dynamics* 30, 455–465.
- Joussaume, S., Braconnot, P., 1997. Sensitivity of paleoclimate simulation results to season definitions. *Journal of Geophysical Research* 102, 1943–1956.
- Jouzel, J., Masson, V., Cattani, O., Falourd, S., Stevenard, M., Stenni, B., Longinelli, A., Johnsen, S.J., Steffensen, J.P., Petit, J.R., Schwander, J., Souchez, R., Barkov, N.I., 2001. A new 27 kyr high resolution East Antarctic climate record. *Geophysical Research Letters* 28, 3199–3202.
- Kaplan, M.R., Wolfe, A.P., 2006. Spatial and temporal variability of Holocene temperature in the North Atlantic region. *Quaternary Research* 65, 223–231.
- Kaufman, D.S., Ager, T.A., Anderson, N.J., Anderson, P.M., Andrews, J.T., Bartlein, P.J., Brubaker, L.B., Coats, L.L., Cwynar, L.C., Duvall, M.L., Dyke, A.S., Edwards, M.E., Eisner, W.R., Gajewski, K., Geirsdóttir, A., Hu, F.S., Jennings, A.E., Kaplan, M.R., Kerwin, M.W., Lozhkin, A.V., MacDonald, G.M., Miller, G.H., Mock, C.J., Oswald, W.W., Otto-Bliesner, B.L., Porinchu, D.F., Ruhland, K., Smol, J.P.,

- Steig, E.J., Wolfe, B.B., 2004. Holocene thermal maximum in the western Arctic (0–180°W). *Quaternary Science Reviews* 23, 529–560.
- Kerwin, M.W., Overpeck, J.T., Webb, R.S., DeVernal, A., Rind, D.H., Healy, R.J., 1999. The role of oceanic forcing in mid-Holocene Northern Hemisphere climatic changes. *Paleoceanography* 14, 200–210.
- Kerwin, M.W., Overpeck, J.T., Webb, R.S., Anderson, K.H., 2004. Pollen-based summer temperature reconstructions for the eastern Canadian boreal forest, subarctic, and Arctic. *Quaternary Science Reviews* 23, 1901–1924.
- Kim, J.H., Schneider, R.R., Mulitza, S., Müller, P.J., 2003. Reconstruction of SE trade-wind intensity based on sea-surface temperature gradients in the Southeast Atlantic over the last 25 kyr. *Geophysical Research Letters* 30, 2144. <http://dx.doi.org/10.1029/2003GL017557>.
- Kim, J.H., Rimbu, N., Lorenz, S.J., Lohmann, G., Nam, S.I., Schouten, S., Rühlemann, C., Schneider, R.R., 2004. North Pacific and North Atlantic sea-surface temperature variability during the Holocene. *Quaternary Science Reviews* 23, 2141–2154.
- Klug, M., Schmidt, S., Bennike, O., Heiri, O., Melles, M., Wagner, B., 2008. Lake sediments from Store Kolbevej, Northeast Greenland, as archive of Late Pleistocene and Holocene climatic and environmental changes. *Boreas* 38, 59–71.
- Langen, P.L., Alexeev, V.A., 2007. Polar amplification as a preferred response in an idealized aquaplanet GCM. *Climate Dynamics* 29, 305–317.
- Leduc, G., Schneider, R., Kim, J.H., Lohmann, G., 2010. Holocene and Eemian sea surface temperature trends as revealed by alkenone and Mg/Ca paleothermometry. *Quaternary Science Reviews* 29, 989–1004.
- Licciardi, J.M., Teller, J.T., Clark, P.U., 1999. Freshwater routing by the Laurentide ice sheet during the last deglaciation. In: Clark, P.U., Webb, R.S., Keigwin, L.D. (Eds.), *Mechanisms of Global Climate Change at Millennial Time Scale*. Geophysical Monograph Series, vol. 112. AGU, Washington, DC, pp. 177–201.
- Ljungqvist, F.C., 2011. The spatio-temporal pattern of the mid-Holocene Thermal Maximum. *Geografie* 116, 91–110.
- Lorenz, S.J., Kim, J.-H., Rimbu, N., Schneider, R.R., Lohmann, G., 2006. Orbitally driven insolation forcing on Holocene climate trends: evidence from alkenone data and climate modelling. *Paleoceanography* 21, PA1002. <http://dx.doi.org/10.1029/2005PA001152>.
- MacDonald, G.M., 2010. Some Holocene palaeoclimatic and palaeoenvironmental perspectives on Arctic/Subarctic climate warming and the IPCC 4th assessment report. *Journal of Quaternary Science* 25, 39–47.
- Marchal, O., Cacho, I., Stocker, T.F., Grimalt, J.O., Cavo, E., Martrat, B., Shackleton, N., Vautravers, M., Cortijo, E., Van Kreveld, S., Anderson, C., Koc, N., Chapman, M., Sbaifi, L., Duplessy, J.C., Sarnthein, M., Turon, J.L., Duprat, J., Jansen, E., 2002. Apparent long-term cooling of the sea surface in the northeast Atlantic and Mediterranean during the Holocene. *Quaternary Science Reviews* 21, 455–483.
- Masson, V., Vimeux, F., Jouzel, J., Morgan, V., Delmotte, M., Ciais, P., Hammer, C., Johnsen, S., Lipenkov, V.Y., Mosley-Thompson, E., Petit, J.-R., Steig, E.J., Stievenaud, M., Vaikmae, R., 2000. Holocene climate variability in Antarctica based on 11 ice-core isotopic records. *Quaternary Research* 54, 348–358.
- Masson-Delmotte, V., Stenni, B., Jouzel, J., 2004. Common millennial-scale variability of Antarctic and Southern Ocean temperatures during the past 5000 years reconstructed from the EPICA Dome C ice core. *The Holocene* 14, 145–151.
- Masson-Delmotte, V., Kageyama, M., Braconnot, P., Charbit, S., Krinner, G., Ritz, C., Guilyardi, E., Jouzel, J., Abe-Ouchi, A., Crucifix, M., Gladstone, R.M., Hewitt, C.D., Kitoh, A., LeGrande, A.N., Marti, O., Merkel, U., Motoi, T., Ohgaito, R., Otto-Bliesner, B., Peltier, W.R., Ross, I., Valdes, P.J., Vettoretti, G., Weber, S.L., Wolk, F., Yu, Y., 2006. Past and future polar amplification of climate change: climate model intercomparisons and ice-core constraints. *Climate Dynamics* 26, 513–529.
- Masson-Delmotte, V., Buiron, D., Ekaykin, A., Frezzotti, M., Gallée, H., Jouzel, J., Krinner, G., Landais, A., Motoyama, H., Oerter, H., Pol, K., Pollard, D., Ritz, C., Schlosser, E., Sime, L.C., Sodemann, H., Stenni, B., Uemura, R., Vimeux, F., 2011. A comparison of the present and last interglacial periods in six Antarctic ice cores. *Climate of the Past* 7, 397–423.
- McCulloch, R.D., Bentley, M.J., Purves, R.S., Hulton, N.R.J., Sugden, D.E., Clapperton, C.M., 2000. Climatic inferences from glacial and palaeoecological evidence at the last glacial termination, southern South America. *Journal of Quaternary Science* 15, 409–417.
- Meehl, G.A., Stocker, T.F., Collins, W.D., Friedlingstein, P., Gaye, A.T., Gregory, J.M., Kitoh, A., Knutti, R., Murphy, J.M., Noda, A., Raper, S.C.B., Watterson, I.G., Weaver, A.J., Zhao, Z.-C., 2007. Global climate projections. In: Solomon, S., Qin, D., Manning, M., Chen, Z., Marquis, M., Averyt, K.B., Tignor, M., Miller, H.L. (Eds.), *Climate Change 2007: the Physical Science Basis*. Contribution of Working Group I to the 4th Assessment Report of the IPCC. Cambridge University Press, Cambridge, United Kingdom.
- Miller, G.H., Brigham-Grette, J., Alley, R.B., Anderson, L., Bauch, H.A., Douglas, M.S.V., Edwards, M.E., Elias, S.A., Finney, B.P., Fitzpatrick, J.J., Funder, S.V., Herbert, T.D., Hinzman, L.D., Kaufman, D.S., MacDonald, G.M., Polyak, L., Robock, A., Serreze, M.C., Smol, J.P., Spielhagen, R., White, J.W.C., Wolfe, A.P., Wolff, E.W., 2010a. Temperature and precipitation history of the Arctic. *Quaternary Science Reviews* 29, 1679–1715.
- Miller, G.H., Alley, R.B., Brigham-Grette, J., Fitzpatrick, J.J., Polyak, L., Serreze, M.C., White, J.W.C., 2010b. Arctic amplification: can the past constrain the future? *Quaternary Science Reviews* 29, 1775–1790.
- Moros, M., Emeis, K., Risebrobakken, B., Snowball, I., Kuijpers, A., McManus, J., Jansen, E., 2004. Sea surface temperatures and ice rafting in the Holocene North Atlantic: climate influences on northern Europe and Greenland. *Quaternary Science Reviews* 23, 2113–2126.
- Neumann, F.H., Scott, L., Bousman, C.B., van As, L., 2010. A Holocene sequence of vegetation change at Lake Eteza, coastal KwaZulu-Natal, South Africa. *Review of Palaeobotany and Palynology* 162, 39–53.
- Nielsen, S.H.H., Koc, N., Crosta, X., 2004. Holocene climate in the Atlantic sector of the Southern Ocean: controlled by insolation or oceanic circulation? *Geology* 32, 317–320.
- Opsteegh, J.D., Haarsma, R.J., Selten, F.M., Kattenberg, A., 1998. ECBILT: a dynamic alternative to mixed boundary conditions in ocean models. *Tellus* 50A, 348–367.
- Osborne, C.P., Mitchell, P.L., Sheehy, J.E., Woodward, F.I., 2000. Modelling the recent historical impacts of atmospheric CO₂ and climate change on Mediterranean vegetation. *Global Change Biology* 6, 445–458.
- Otto, J., Raddatz, T., Claussen, M., Brovkin, V., Gayler, V., 2009. Separation of atmosphere-ocean-vegetation feedbacks and synergies for mid-Holocene climate. *Geophysical Research Letters* 36, L09701. <http://dx.doi.org/10.1029/2009GL037482>.
- Peltier, W.R., 2004. Global glacial isostasy and the surface of the ice-age Earth: the ICE-5G (VM2) model and GRACE. *Annual Review of Earth and Planetary Sciences* 32, 111–149.
- Petoukhov, V., Claussen, M., Berger, A., Crucifix, M., Eby, M., Eliseev, A.V., Fichet, T., Ganopolski, A., Goosse, H., Kamenkovich, I., Mokhov, I.I., Montoya, M., Mysak, L.A., Sokolov, A., Stone, P., Wang, Z., Weaver, A.J., 2005. EMIC Inter-comparison Project (EMIP-CO₂): comparative analysis of EMIC simulations of climate, and of equilibrium and transient responses to atmospheric CO₂ doubling. *Climate Dynamics* 25, 363–385.
- Potito, A.P., Porinchi, D.F., MacDonald, G.M., Moser, K.A., 2006. A late Quaternary chronomid-inferred temperature record from the Sierra Nevada, California, with connections to northeast Pacific sea surface temperatures. *Quaternary Research* 66, 356–363.
- Raynaud, D., Barnola, J.-M., Chappellaz, J., Blunier, T., Indermühle, A., Stauffer, B., 2000. The ice record of greenhouse gases: a view in the context of future changes. *Quaternary Science Reviews* 19, 9–17.
- Renssen, H., Goosse, H., Fichet, T., 2002. Modeling the effect of freshwater pulses on the early Holocene climate: the influence of high frequency climate variability. *Paleoceanography* 17, 1020. <http://dx.doi.org/10.1029/2001PA000649>.
- Renssen, H., Seppä, H., Heiri, O., Roche, D.M., Goosse, H., Fichet, T., 2009. The spatial and temporal complexity of the Holocene Thermal Maximum. *Nature Geoscience* 2, 411–414.
- Renssen, H., Goosse, H., Crosta, X., Roche, D.M., 2010. Early Holocene Laurentide Ice Sheet deglaciation causes cooling in the high-latitude Southern Hemisphere through oceanic teleconnection. *Paleoceanography* 25, PA3204. <http://dx.doi.org/10.1029/2009PA001854>.
- Rimbu, N., Lohmann, G., Lorenz, S.J., Kim, J.H., Schneider, R.R., 2004. Holocene climate variability as derived from alkenone sea surface temperature and coupled ocean-atmosphere model experiments. *Climate Dynamics* 23, 215–227.
- Roberts, S.J., Hodgson, D.A., Bentley, M.J., Smith, J.A., Millar, I., Olive, V., Sugden, D.E., 2008. The Holocene history of George VI Ice Shelf, Antarctic Peninsula from clast-provenance analysis of epishelf lake sediments. *Palaeogeography, Palaeoclimatology, Palaeoecology* 259, 258–283.
- Salonen, J.S., Seppä, H., Väiranta, M., Jones, V.J., Self, A., Heikkilä, M., Kultti, S., Yang, H., 2011. The Holocene thermal maximum and late-Holocene cooling in the tundra of NE European Russia. *Quaternary Research* 75, 501–511.
- Seppä, H., Bjune, A.E., Telford, R.J., Birks, H.J.B., Veski, S., 2009. Last nine-thousand years of temperature variability in northern Europe. *Climate of the Past* 5, 523–535.
- Shevenell, A.E., Ingalls, A.E., Domack, E.W., Kelly, C., 2011. Holocene southern ocean surface temperature variability west of the Antarctic Peninsula. *Nature* 470, 250–254.
- Shi, Y.F., Kong, Z.C., Wang, S.M., Tang, L.Y., Wang, F.B., Yao, T.D., Zhao, X.T., Zhang, P.Y., Shi, S.H., 1992. Climatic variations and important events of Holocene megathermal in China (in Chinese). *Scientia Sinica Series B* 12, 1300–1308.
- Sjunneskog, C., Taylor, F., 2002. Postglacial marine diatom record of the Palmer deep, Antarctic Peninsula (ODP Leg 178, Site 1098) 1. Total diatom abundance. *Paleoceanography* 17. <http://dx.doi.org/10.1029/2000PA000563>.
- Stott, L., Cannariato, K., Thunnell, R., Haug, G.H., Koutavas, A., Lund, S., 2004. Decline of surface temperature and salinity in the western tropical Pacific Ocean in the Holocene epoch. *Nature* 431, 56–59.
- Swann, G.E.A., Leng, M.J., Juschus, O., Melles, M., Brigham-Grette, J., Sloane, H.J., 2010. A combined oxygen and silicon diatom isotope record of Late Quaternary change in Lake El'gygytgyn, North East Siberia. *Quaternary Science Reviews* 29, 774–786.
- Taylor, F., Whitehead, J., Domack, E., 2001. Holocene paleoclimate change in the Antarctic Peninsula: evidence from the diatom, sedimentary and geochemical record. *Marine Micropaleontology* 41, 25–43.
- Thomas, E.R., Wolff, E.W., Mulvaney, R., Steffensen, J.P., Johnsen, S.J., Arrowsmith, C., White, J.W.C., Vaughn, B., Popp, T., 2007. The 8.2 ka event from Greenland ice cores. *Quaternary Science Reviews* 26, 70–81.
- Viau, A.E., Gajewski, K., 2009. Reconstructing millennial-scale, regional Paleoclimates of boreal Canada during the Holocene. *Journal of Climate* 22, 316–333.
- Viau, A.E., Gajewski, K., Sawada, M.C., Fines, P., 2006. Millennial-scale temperature variations in during the Holocene. *Journal of Geophysical North America Research* 111, D09102. <http://dx.doi.org/10.1029/2005JD006031>.
- Vinther, B.M., Buchardt, S.L., Clausen, H.B., Dahl-Jensen, D., Johnsen, S.J., Fisher, D.A., Koerner, R.M., Raynaud, D., Lipenkov, V., Andersen, K.K., Blunier, T.,

- Rasmussen, S.O., Steffensen, J.P., Svensson, A.M., 2009. Holocene thinning of the Greenland ice sheet. *Nature* 461, 385–388.
- Wagner, B., Melles, M., 2007. The heterogeneity of Holocene climatic and environmental history along the East Antarctic coastal regions. In: Cooper, A.K., Raymond, C.R. (Eds.), *In Antarctica: a Keystone in a Changing World – Online Proceedings of the 10th ISAES*, USGS Open-File Report 2007-1047, Extended Abstract 161, 4 p.
- Waldmann, N., Ariztegui, D., Anselmetti, F.S., Austin Jr., J.A., Moy, C.M., Stern, C., Recasens, C., Dunbar, R.B., 2010. Holocene climatic fluctuations and positioning of the Southern Hemisphere westerlies in Tierra del Fuego (54°S), Patagonia. *Journal of Quaternary Science* 25, 1063–1075.
- Wang, Y., Cheng, H., Edwards, R.L., He, Y., Kong, X., An, Z., Wu, J., Kelly, M.J., Dykoski, C., Li, X., 2005. The Holocene Asian Monsoon: links to solar changes and North Atlantic climate. *Science* 308, 854–857.
- Wanner, H., Beer, J., Butikofer, J., Crowley, T.J., Cubasch, U., Fluckiger, J., Goosse, H., Grosjean, M., Joos, F., Kaplan, J.O., Kuttel, M., Muller, S.A., Prentice, I.C., Solomina, O., Stocker, T.F., Tarasov, P., Wagner, M., Widmann, M., 2008. Mid- to Late Holocene climate change: an overview. *Quaternary Science Reviews* 27, 1791–1828.
- Weber, S.L., Crowley, T.J., van der Schrier, G., 2004. Solar irradiance forcing of centennial climate variability during the Holocene. *Climate Dynamics* 24, 539–553.
- Weldeab, S., Lea, D.W., Schneider, R.R., Andersen, N., 2007. 155,000 years of West African monsoon and ocean thermal evolution. *Science* 316, 1303–1307.
- Williams, P.W., King, D.N.T., Zhao, J.X., Collerson, K.D., 2004. Speleothem master chronologies: combined Holocene ^{18}O and ^{13}C records from the North Island of New Zealand and their palaeoenvironmental interpretation. *The Holocene* 14, 194–208.
- Wilmshurst, J.M., McGlone, M.S., Leathwick, J.R., Newnham, R.M., 2007. A pre-deforestation pollen-climate calibration model for New Zealand and quantitative temperature reconstructions for the past 18 000 years BP. *Journal of Quaternary Science* 22, 535–547.
- Xia, Q., Zhao, J.X., Collerson, K.D., 2001. Early-Mid Holocene climatic variations in Tasmania, Australia: multi-proxy records in a stalagmite from Lynds Cave. *Earth and Planetary Science Letters* 194, 177–187.
- Xiao, J., Nakamura, T., Lu, H., Zhang, G., 2002. Holocene climate changes over the desert/loess transition of north-central China. *Earth and Planetary Science Letters* 197, 11–18.
- Zhang, Q., Sundqvist, H.S., Moberg, A., Körnich, H., Nilsson, J., Holmgren, K., 2010. Climate change between the mid and late Holocene in northern high latitudes – Part 2: model-data comparisons. *Climate of the Past* 6, 609–626.
- Zhao, Y., Yu, Z., Zhao, W., 2011. Holocene vegetation and climate histories in the eastern Tibetan Plateau: controls by insolation-driven temperature or monsoon-derived precipitation changes? *Quaternary Science Reviews* 30, 1173–1184.